

# Dynamics of ion-ion plasmas under radio frequency bias

Vikas Midha<sup>a)</sup> and Demetre J. Economou<sup>b)</sup>

*Plasma Processing Laboratory, Department of Chemical Engineering, University of Houston, Houston, Texas 77204-4792*

(Received 10 October 2000; accepted for publication 4 May 2001)

A time-dependent one-dimensional fluid model was developed to study the dynamics of a positive ion-negative ion (ion-ion) plasma under the influence of a rf bias voltage. The full ion momentum and continuity equations were coupled to the Poisson equation for the electrostatic field. Special emphasis was placed on the effect of applied bias frequency. Due to the lower temperature and greater mass of negative ions compared to electrons, the sheath structure in ion-ion plasmas differs significantly from that of conventional electron-ion plasmas, and shows profound structure changes as the bias frequency is varied. For low bias frequencies (100 kHz), the charge distribution in the sheath is monotonic (switching from positive to negative) during each half cycle. For intermediate frequencies (10 MHz), when the bias period approaches the ion transit time through the sheath, double layers form with both positive and negative charges coexisting in the sheath. For high frequencies (60 MHz), beyond the plasma frequency, plasma waves are launched from the sheath edge, and the sheath consists of multiple peaks of positive and negative charge (multiple double layers). For a relatively large range of bias frequencies (up to the plasma frequency), each electrode is bombarded *alternately* by high energy positive and negative ions during a rf bias cycle. For bias frequencies greater than the plasma frequency, however, the electrode is bombarded simultaneously by low energy positive and negative ions with ion energies approaching the thermal value. The ion energy was found to increase with the applied bias potential. Also, at relatively high pressures (20 mTorr), the ion energy at low frequencies (100 kHz) is limited by collisions. The peak ion energy may then be increased by using an intermediate bias frequency (10 MHz). At lower pressures, however, the effect of collisions is mitigated while the effect of ion transit time becomes significant as the bias frequency increases. In this case, a low bias frequency (100 s of kHz) is favorable for extracting high energy ions from the plasma. © 2001 American Institute of Physics.

[DOI: 10.1063/1.1383260]

## I. INTRODUCTION

Ion-ion plasmas are plasmas that consist of positive and negative ions only (electron-free plasmas). In practice, a small number of electrons can coexist, provided that the dominant negative charge carriers are negative ions; see Ref. 1 for quantification. Ion-ion plasmas may be formed in the afterglow of pulsed discharges in electronegative gases.<sup>2–5</sup> Simulations of a pulsed chlorine discharge, for example,<sup>1</sup> showed that once the power is switched off, the electron density decays rapidly as a function of time due to diffusion and dissociative attachment with neutral molecules. In the presence of a significant number of electrons, negative ions remain trapped in the reactor due to the electrostatic fields, and are unable to diffuse to the walls. Therefore, while the average electron density drops in the afterglow, the average negative ion density increases due to dissociative attachment. Thus, the plasma becomes increasingly electronegative as a function of time in the afterglow. Eventually, there is a transition to an ion-ion plasma<sup>1–6</sup> when the electron density and temperature are low enough that negative ions become the dominant negative charge carrier in the plasma. This state is

characterized by such weak electrostatic fields that negative ions are now able to diffuse to the walls. Thus, in contrast to electron-ion plasmas, it is possible to extract negative ions out of an ion-ion plasma.

The electrostatic fields in an ion-ion plasma are determined by ions instead of electrons. In conventional electron-ion plasmas, the reason of existence of electrostatic fields is to balance wall losses of the lighter and more energetic electrons out of the plasma with those of the heavier and colder positive ions. However, by replacing electrons with negative ions in the plasma, the mass and temperature of the negatively charged and positively charged species become comparable. Ion-ion plasmas, therefore, are characterized by much weaker electrostatic fields, with a plasma potential of the order of the ion temperature (without external bias). In the ideal case of a positive ion-negative ion plasma in which both ion species have equal masses and temperatures, ion-ion plasmas are characterized by the absence of electrostatic fields and the absence of sheaths (when no bias voltage is applied). The spatial profiles of positive and negative ions coincide throughout the length of the reactor, and both ions are able to diffuse *freely* to the walls. Other salient features of ion-ion plasmas include:<sup>7–10</sup> (a) only heavy particles participate in plasma chemistry, (b) the plasma impedance can be changed drastically by light irradiation (negative ion pho-

<sup>a)</sup>Currently with General Electric-CRD, Schenectady, NY 12065.

<sup>b)</sup>Author to whom all correspondence should be addressed; electronic mail: economou@uh.edu

todetachment) that creates electrons, (c) the potential distribution in an ion-ion plasma (without a bias or with a low frequency bias) behaves as in liquid electrolytes,<sup>11</sup> (d) ion-ion plasma properties can be measured by a Langmuir probe.<sup>12</sup>

It is also possible to form ion-ion plasmas (with a small number of electrons) under steady state conditions by operating a strongly electronegative discharge at relatively high pressure.<sup>13–15</sup> When the ratio of negative ion to electron density (electronegativity) becomes greater than about 1000, electrons do not play a significant role and negative ion extraction should be possible.<sup>1,2</sup> An ion-ion plasma (with a small number of electrons) can coexist in the same vessel with a conventional electron-ion plasma.<sup>14–16</sup> The transition between the two plasmas can be smooth, or double layers may separate the two plasmas.<sup>17–20</sup>

Ion-ion plasmas offer unique possibilities for plasma etching applications. In contrast to conventional electron-ion plasmas in which negative ions remain trapped in the bulk plasma, negative ions can participate in etching in ion-ion plasmas,<sup>21–24</sup> possibly reducing charging damage and etch-profile distortions associated with electron-ion plasma etching.<sup>25</sup> Ion-ion plasmas are also important in negative ion sources,<sup>26,27</sup> the *D* layer of the atmosphere,<sup>28</sup> and in dusty plasmas.<sup>10</sup>

As mentioned above, an ideal (two ions with equal masses and temperatures) ion-ion plasma without an applied external bias potential is characterized by the absence of electrostatic fields and free diffusion of ions to the walls. The profile of positive-ion density simply overlaps with that of the negative-ion density. In the presence of a bias potential, however, the positive and negative ions separate to form a sheath near the electrode. In this article, the influence of an external rf bias on an ion-ion plasma is examined. A time-dependent one-dimensional fluid model is developed which resolves the sheath regions near the electrodes. The model includes the Poisson equation for the electrostatic field coupled with the continuity and momentum equations for the ion density and velocity, respectively. The effect of varying the bias frequency, bias potential and operating pressure on the dynamics of the plasma, and the flux and energy of ions bombarding the electrode are examined. Although the spatiotemporal dynamics of conventional electron-ion plasmas have been studied extensively,<sup>29–32</sup> we are not aware of any published reports on the dynamics of ion-ion plasmas under the influence of an external rf bias voltage.

## II. MODEL DEVELOPMENT

A low-pressure ion-ion plasma formed in the late afterglow of a pulsed chlorine discharge is considered. The model assumptions are outlined below.

(1) A high degree of gas dissociation is assumed. Thus, the only ions present are  $\text{Cl}^+$  and  $\text{Cl}^-$  both at an ion temperature of 300 K.

(2) The electron density is assumed to have decayed to low enough values compared to the ion density (electronegativity greater than 1000) so that the presence of electrons may be completely neglected. Similarly, any electrons which

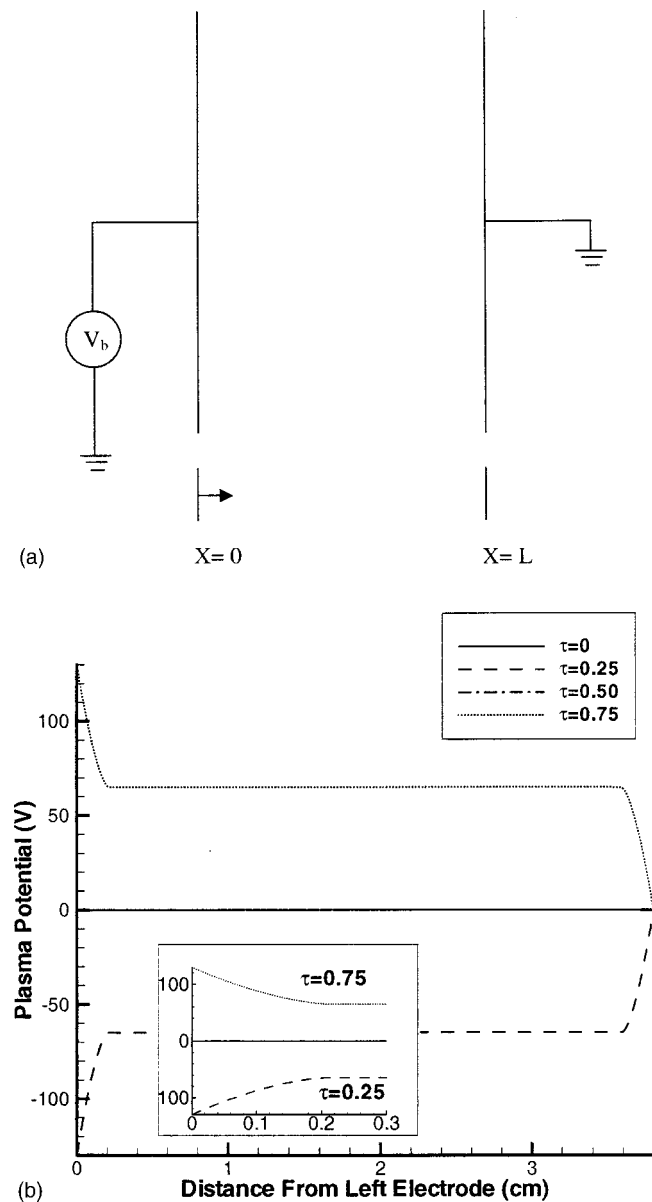


FIG. 1. (a) Schematic of the one-dimensional parallel plate system considered. (b) Spatiotemporal evolution of the potential at base case conditions for a bias frequency of 100 kHz.

may be generated due to capacitive coupling under the applied bias are neglected.

(3) The parallel electrodes are assumed to be of equal area (one-dimensional system). A sinusoidal bias voltage is applied to the driven (left) electrode, while the other (right) electrode is grounded [Fig. 1(a)].

## A. Governing equations

A one-dimensional fluid model for an ion-ion plasma under the influence of an externally applied bias potential is developed. The model consists of the following set of governing equations: The continuity equation for the positive and negative ions is given by

$$\frac{\partial n_i}{\partial t} = -\frac{\partial}{\partial x}(n_i u_i) + R_i, \quad (1)$$

where  $n_i$  is the ion density,  $u_i$  is the ion fluid velocity, and  $R_i$  represents the rate of generation or loss of ions through chemical reaction (ion-ion recombination in our case, with rate coefficient of  $5 \times 10^{-8} \text{ cm}^3/\text{s}$ );  $i=p$  and  $i=n$  for positive and negative ions, respectively. The ion fluid velocities are computed by the momentum balance equations:

$$\frac{\partial(n_i u_i)}{\partial t} + \frac{\partial(n_i u_i u_i)}{\partial x} = \left(\frac{s_i q}{M_i}\right) n_i E - \left(\frac{k T_i}{M_i}\right) \frac{\partial n_i}{\partial x} - n_i u_i \nu_i, \quad (2)$$

where  $M_i$  is the ion mass,  $T_i$  is the ion temperature,  $\nu_i$  is the ion-neutral collision frequency,  $s_i$  is the charge number of the ion, and  $q$  is the value of the elementary charge. The terms in Eq. (2) (from left to right) represent the time rate of change in ion momentum or temporal inertia, spatial inertia, electrostatic force, pressure gradient, and collisional drag, respectively. The ion-neutral collision frequency was taken as proportional to the ion velocity (low pressure constant mean free path case, see Ref. 15). The electrostatic field is governed by the Poisson equation:

$$\frac{\partial E}{\partial x} = \frac{q}{\epsilon_0} (n_p - n_n), \quad (3)$$

where the electric field,  $E$ , is related to the plasma potential,  $V$ , by  $E = -\partial V / \partial x$ . Here  $\epsilon_0$  is the permittivity of free space. The potential at the driven (left,  $x=0$ ) electrode is assumed to be of the form

$$V(x=0) = V_b \sin(\omega t), \quad (4)$$

where  $V_b$  is the amplitude and  $\omega$  is the frequency of the applied bias. The potential at the grounded (right,  $x=L$ ) electrode is fixed at zero [Fig. 1(a)].

The governing equations of the fluid model, therefore, consist of two continuity equations for ion densities  $n_p$  and  $n_n$ , two momentum equations for ion velocities  $u_p$  and  $u_n$  and the Poisson equation for the electrostatic field. Initial conditions were: identical positive and negative ion density profiles as obtained in an ion-ion plasma with equal mass and temperature of the ions (nearly parabolic if ion-ion recombination is slow) with a peak ion density of  $10^{11} \text{ cm}^{-3}$ , and potential equal to zero everywhere. Boundary conditions included zero positive ion density on the walls.

## B. Linear analysis (Ref. 33)

A preliminary analysis of the system of equations is instructive to estimate the time scales of important physical processes. First, the time scale for ion-ion recombination for a peak ion density of  $10^{11} \text{ cm}^{-3}$  is long compared to other physical processes and is neglected in this analysis, i.e.,  $R_i = 0$ . If, in addition, a constant ion collision frequency is assumed for the moment, Eqs. (1) and (2) may be combined to yield the following equation for ion density:

$$\begin{aligned} \frac{\partial^2 n_i}{\partial t^2} + \nu_i \frac{\partial n_i}{\partial t} &= -\frac{\partial^2(n_i u_i^2)}{\partial x^2} - \left(\frac{s_i q}{M_i}\right) \frac{\partial(n_i E)}{\partial x} \\ &\quad + \left(\frac{k T_i}{M_i}\right) \frac{\partial^2 n_i}{\partial x^2}. \end{aligned} \quad (5)$$

This equation shows the nonlinear nature of ion transport in the plasma. The nonlinearities are due to spatial inertia [third term from the left hand side in Eq. (5)] and electrostatic fields (fourth term). Assuming an initially flat density profile ( $n_p = n_n = n_0$ ) and small perturbations of that density, Eq. (5) may be linearized to give

$$\frac{\partial^2 n_p}{\partial t^2} + \nu_i \frac{\partial n_p}{\partial t} = -\left(\frac{n_0 q}{M_i}\right) \frac{\partial E}{\partial x} + \left(\frac{k T_i}{M_i}\right) \frac{\partial^2 n_p}{\partial x^2}, \quad (6)$$

for the positive-ion density and

$$\frac{\partial^2 n_n}{\partial t^2} + \nu_i \frac{\partial n_n}{\partial t} = +\left(\frac{n_0 q}{M_i}\right) \frac{\partial E}{\partial x} + \left(\frac{k T_i}{M_i}\right) \frac{\partial^2 n_n}{\partial x^2}, \quad (7)$$

for the negative-ion density. Equations (6) and (7) may now be combined to identify two modes of propagation.

(a) The total density ( $n_p + n_n$ ), evolves according to the relation

$$\frac{\partial^2(n_p + n_n)}{\partial t^2} + \nu_i \frac{\partial(n_p + n_n)}{\partial t} = \left(\frac{k T_i}{M_i}\right) \frac{\partial^2(n_p + n_n)}{\partial x^2}. \quad (8)$$

For time scales greater than the characteristic collision time ( $\tau_c = 1/\nu_i$ ), temporal inertia is negligible and Eq. (8) reduces to

$$\frac{\partial(n_p + n_n)}{\partial t} = D_i \frac{\partial^2(n_p + n_n)}{\partial x^2}, \quad (9)$$

where  $D_i$  is the ion diffusivity given by  $D_i = (k T_i / \nu_i M_i)$ . Therefore, over relatively long time scales, the overall density of an ion-ion plasma simply decays due to ion diffusion and is independent of the applied bias potential and frequency. Of course, over even longer time scales, ion-ion recombination (nonlinear term) enters the picture.

For time scales shorter than the characteristic collision time  $\tau_c$ , temporal inertia is dominant and Eq. (9) reduces to

$$\frac{\partial^2(n_p + n_n)}{\partial t^2} = c_i^2 \frac{\partial^2(n_p + n_n)}{\partial x^2}, \quad (10)$$

where  $c_i$  is the ion sonic velocity given by  $c_i = \sqrt{k T_i / M_i}$ . Equation (10) represents the propagation of ion-acoustic waves. In ion-ion plasmas, ion acoustic waves propagate slowly due to the thermal motion of the ions, whereas in electron-ion plasmas, ion-acoustic waves can also propagate due to the presence of electrostatic fields, which are governed by the electron temperature. Therefore, the sonic velocity of ions is significantly lower in ion-ion plasmas compared to electron-ion plasmas, since the electron temperature is normally much greater than the ion temperature.

(b) The other mode of propagation obtained from Eqs. (6) and (7) is the charge density ( $n_p - n_n$ ), which propagates according to the relation

TABLE I. Base case parameter values used in the simulation.

Peak ion density	$10^{11} \text{ cm}^{-3}$
Ion temperature	0.026 eV
Ion mass	35.5 amu
Pressure	20 mTorr
Bias potential (peak to peak)	130 V

$$\frac{\partial^2(n_p - n_n)}{\partial t^2} + \nu_i \frac{\partial(n_p - n_n)}{\partial t} = -2 \left( \frac{qn_0}{M_i} \right) \frac{\partial E}{\partial x} + \left( \frac{kT_i}{M_i} \right) \frac{\partial^2(n_p - n_n)}{\partial x^2}. \quad (11)$$

For long time scales compared to  $\tau_c$ , Eq. (11) reduces to

$$\frac{\partial(n_p - n_n)}{\partial t} = -(2\mu_i n_0) \frac{\partial E}{\partial x} + D_i \frac{\partial^2(n_p - n_n)}{\partial x^2}, \quad (12)$$

where  $\mu_i = (q/\nu_i M_i)$  is the ion mobility. Equation (12) gives the rate of decay of charge density due to ion drift and ion diffusion. Since the time scales for ion drift and ion diffusion are significantly less than those associated with electrons, the charge density decays at a much slower rate in an ion-ion plasma compared to an electron-ion plasma.

For short time scales compared to  $\tau_c$ , Eq. (11) reduces to

$$\frac{\partial^2(n_p - n_n)}{\partial t^2} = -\omega_i^2(n_p - n_n) + \left( \frac{kT_i}{M_i} \right) \frac{\partial^2(n_p - n_n)}{\partial x^2}, \quad (13)$$

where  $\omega_i = (2q^2 n_0 / \epsilon_0 M_i)$  is an ion-plasma frequency. Equation (13) was derived by substituting Eq. (3) for the electric field gradient into Eqs. (6) and (7). Equation (13) represents propagation of plasma or Langmuir waves in an ion-ion plasma. These plasma waves are similar in nature to the plasma waves in electron-ion plasmas and represent oscillations in charge density due to electrostatic fields and particle inertia. For frequencies greater than the plasma frequency, these oscillations in charge density propagate in space due to thermal motion to produce a plasma wave. For frequencies less than the plasma frequency, the oscillations are unable to propagate in space and decay within a few Debye lengths. Since the ion-plasma frequency is significantly less than the electron-plasma frequency, plasma waves may be present in ion-ion plasmas even for relatively low-frequency perturbations.

Table I shows the parameter values used as a base case in this study and Table II summarizes the important time scales which emerge from the linear analysis. The response of an ion-ion plasma to a rf bias may be divided into different regimes based on the characteristic time scale for collisions and the ion plasma frequency. Over long time scales compared to the collision time, the total density in the bulk plasma decays simply due to ion diffusion [Eq. (10)] and is unaffected by the presence of the applied bias. Similarly for long-time scales, the evolution of charge in the sheath regions will evolve simply due to ion drift and ion diffusion [Eq. (12)]. For short-time scales compared to the collision time, the sheaths become collisionless and the time scale

TABLE II. Time scales of important physical process.

Collision frequency $\nu_i$ (evaluated at $u_i = c_i$ )	300 kHz
Frequency of ion diffusion across discharge length ( $L = 3.8 \text{ cm}$ )	1 kHz
Frequency of ion drift across sheath thickness ( $L_s = 0.2 \text{ cm}$ )	3 MHz
Frequency of ion diffusion across sheath thickness ( $L_s = 0.2 \text{ cm}$ )	75 kHz
Plasma frequency $\omega_{pi}$ (evaluated at sheath edge $n_i = 10^{10} \text{ cm}^{-3}$ )	30 MHz

corresponding to the ion-plasma frequency is important. If the time period of the bias is greater than the ion-plasma frequency, the ion-plasma frequency determines the time scale over which quasineutrality is restored. Therefore, the ion-plasma frequency is a measure of the transit time of the ions through the sheath and may be expressed as

$$\omega_i = \frac{u_{av}}{L_s} = \sqrt{\frac{\left( \frac{qV_b}{M_i} \right)}{\left( \frac{\epsilon_0 V_b}{2qn_0} \right)}}, \quad (14)$$

where  $u_{av}$  is a characteristic velocity of ions in the sheath and  $L_s$  is a characteristic distance (sheath thickness) over which charge separation occurs. Similarly, for time periods less than the plasma frequency, there is insufficient time for quasineutrality to be restored and plasma waves may be launched.

Although linear analysis provides much physical insight, linear analysis cannot be used to provide quantitative information on the dynamics of ion-ion plasmas. This is due to the following reasons:

(1) Linear analysis is valid only for small perturbations in the ion density with an initially uniform profile. However, the ion-ion plasma formed in the afterglow is initially non-uniform with a maximum at the center and a minimum at the electrodes. Consequently, the ion plasma frequency is not constant but varies spatially along the length of the reactor. The ion plasma frequency is lowest at the electrode and increase significantly towards the center.

(2) Application of a bias potential results in large perturbations in the charge density since the magnitude of the applied potential for practical interest is several orders of magnitude greater than the ion temperature. Therefore, perturbations in the ion density are of the order of the density itself and cannot be considered small. Also, the contribution of the electrostatic field [fourth term from left in Eq. (5)] is nonlinear.

(3) At low pressures, the collision frequency is not constant; a constant mean free path is a better approximation. For length scales less than the mean free path, the nonlinearity due to spatial inertia [third term from left in Eq. (5)] becomes significant. The collision frequency is a function of the ion velocity and the collisional drag term in the momentum equations also becomes nonlinear. For these reasons, a numerical solution of the governing Eqs. (1)–(3) is required to obtain quantitative results.

### III. NUMERICAL METHOD

The governing system of Eqs. (1)–(3) was discretized in space using a finite-difference scheme based on a staggered mesh.<sup>34</sup> Ion densities and plasma potential were evaluated on one set of grid points while other dependent quantities (including ion velocities, fluxes, and electric field) were evaluated on a staggered set of grid points. Upwind-biased finite-difference operators were employed to approximate the spatial inertia terms in the ion momentum equations. Discretization in space converted the original set of Eqs. (1)–(3) into a time-dependent differential-algebraic equation (DAE) system. This set of DAEs was solved using LSODI, a fully implicit, variable order, variable time step integrator based on backward difference formulas.<sup>35</sup> A nonuniform mesh of 301 grid points biased towards the sheaths near the electrodes was employed. Typical CPU times for each run were about 10–20 min on a 125 MHz Unix workstation depending on the bias frequency. In order to obtain a periodic solution, only a few cycles were required for low bias frequencies, whereas 100s of cycles were required for high bias frequencies.

### IV. RESULTS AND DISCUSSION

Based on the preliminary linear analysis, the ion-ion plasma response to an applied rf bias may be divided into three regimes depending on the frequency of the applied bias  $\omega$ , the characteristic ion collision frequency  $\nu_i$ , and the ion plasma frequency  $\omega_i$ , the latter evaluated at the sheath edge. In all figures below,  $\tau$  is the dimensionless bias period; for  $0 < \tau < 0.5$  the bias applied to the left electrode is negative, and for  $0.5 < \tau < 1$ , the bias applied to the left electrode is positive [Fig. 1(a)]. All results refer to the base case conditions (Table I) unless stated otherwise.

#### A. Low frequency regime ( $\omega < \nu_i < \omega_i$ )

At low bias frequencies, the bias period is greater than the characteristic time scale for collisions. Therefore, collisional drag dominates over temporal inertia and the ion velocity is in quasisteady state with respect to the local electric field. In this regime, the bias period is also greater than the transit time of the ions through the sheath and the ions are able to respond faithfully to the instantaneous value of applied bias without a significant phase lag.

The spatiotemporal potential distribution between the plates is shown in Fig. 1(b) for a bias frequency of 100 kHz. In contrast to electron-ion plasmas, in which the plasma potential is the most positive potential in the system, the spatial potential profile in ion-ion plasmas is monotonic and is symmetrically distributed between the two electrodes. This symmetry is a direct consequence of the equal masses and temperatures of the positively and negatively charged species assumed for this particular ion-ion plasma. Such monotonic potential profiles are found in liquid electrolyte systems where the mass and temperature of positive and negative ions are comparable as well. At any instant in time, one electrode acquires a net positive potential with respect to the bulk plasma while the other electrode acquires an equal negative potential. During the period  $\tau = 0 - 0.5$  the left elec-

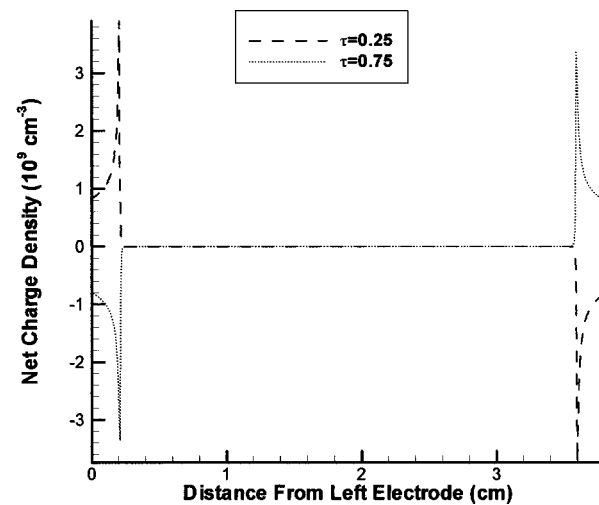


FIG. 2. Spatiotemporal evolution of net charge at base case conditions for a bias frequency of 100 kHz.

trode ( $x=0$ ) is negatively biased with respect to the bulk plasma while the right electrode ( $x=L$ ) is positively biased. Similarly during the period 0.5–1.0, the left electrode becomes positively biased while the right electrode becomes negatively biased with respect to the bulk plasma. At this low frequency, the displacement current is negligible compared to the conduction current in the bulk plasma and most of the potential drop occurs in the sheaths near the electrodes. This potential profile of Fig. 1(b) is related to the evolution of charge density in the ion-ion sheaths formed at the two electrodes.

Figure 2 shows the spatial profiles of the net charge density at  $\tau=0.25$  and 0.75. During each half of the bias cycle, positive ions are attracted towards the negatively biased electrode while negative ions are repelled. This results in the formation of a sheath with a net positive charge at the negatively biased electrode. Conversely, negative ions are attracted towards the positively biased electrode while the positive ions are repelled. This results in the formation of a sheath with a net negative charge at the positively biased electrode. Therefore, in contrast to electron-ion plasmas, in which the sheaths contain a net positive charge, the electrode sheaths in ion-ion plasmas contain equal and opposite net charges. The polarity of the charge in each sheath is reversed during each half cycle of the rf bias.

Figures 3 and 4 show, respectively, the evolution of the positive and negative ion-density profiles near the left electrode during the second half of a bias cycle ( $0.5 < \tau < 1$ ). The left electrode was previously ( $0 < \tau < 0.5$ ) negatively biased with respect to the bulk plasma, has no net bias at  $\tau=0.5$  and remains positively biased through the second half of the cycle. At  $\tau=0.5$ , both positive and negative ions diffuse towards the electrode as the electrode potential is equal to the plasma potential. Since the bias period is comparable to the characteristic diffusion time of ions through the sheath (Table II), the sheath does not have sufficient time to completely collapse by  $\tau=0.5$  and a relatively small positive charge persists in the sheath from the previous half cycle. The electrostatic field due to this charge is responsible for

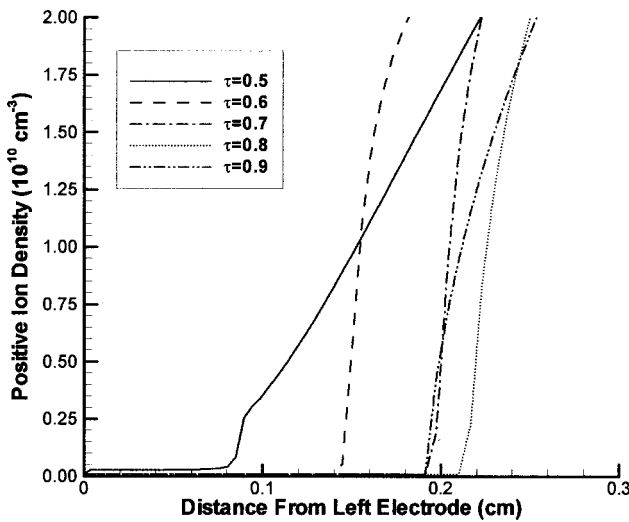


FIG. 3. Spatiotemporal evolution of positive ion density near left electrode at base case conditions for a bias frequency of 100 kHz.

small fronts in the ion-density profiles at the sheath edge at  $x=0.08$  cm. Similarly, the potential in Fig. 1(b) is not constant for all spatial locations at  $\tau=0.5$  and shows the formation of minor peaks in the sheath regions [small blips in Fig 1(b), at  $\tau=0$  and 0.5]. This effect is small at low operating frequencies but becomes significant at higher frequencies and will be addressed in more detail in the following sections.

After  $\tau=0.5$ , the electrode potential increases with time and negative ions are attracted towards the electrode while positive ions are repelled away from the electrode. Therefore, the sheath acquires a net negative charge. A front in the positive-ion density profile is formed (Fig. 3) which represents a competition between repulsion due to the electrostatic field (ion drift) and ion diffusion towards the electrode. As the electrode potential increases, this front is gradually displaced away from the electrode towards the bulk plasma resulting in an increase in the sheath width.

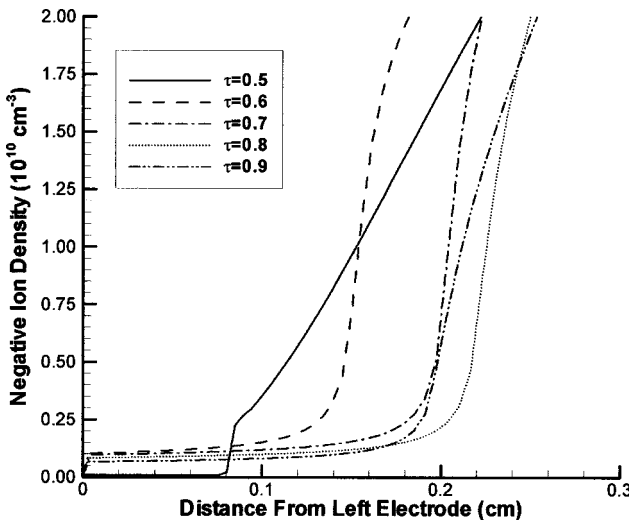


FIG. 4. Spatiotemporal evolution of negative ion density near left electrode at base case conditions for a bias frequency of 100 kHz.

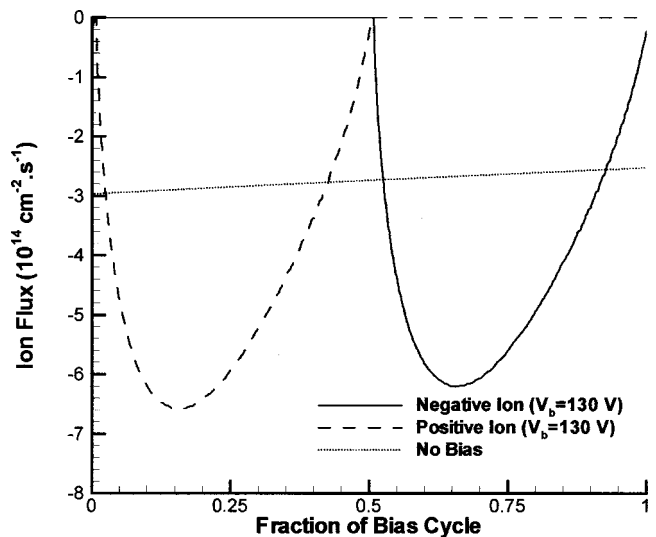


FIG. 5. Ion flux at the left electrode during a bias cycle at base case conditions for a bias frequency of 100 kHz.

The electrode potential decreases during the last quarter of the cycle ( $\tau=0.75$ –1.0), the electrostatic field weakens and the positive-ions begin to diffuse back towards the electrode (Fig. 3,  $\tau=0.9$ ). The sheath width gradually shrinks as the magnitude of the bias potential decreases. As in the case of  $\tau=0.5$ , the positive and negative ions are unable to diffuse back fully to the electrode at  $\tau=1.0$ . Therefore, the sheath does not fully collapse and a small negative charge persists in the sheaths for the next cycle. The sheath at the right electrode also shows similar behavior but is  $180^\circ$  out of phase with respect to the sheath at the left electrode.

Figure 5 shows the evolution of the ion fluxes at the left electrode during a bias cycle. For this low operating frequency, the left electrode is bombarded alternately by positive ions and negative ions during each half of the bias cycle. This is in agreement with experimental data.<sup>36</sup> The peak in the negative-ion flux is slightly less than the peak in the positive-ion flux due to continuous depletion of the plasma (no ionization in the ion-ion plasma). At this relatively low operating frequency, a significant fraction of the plasma is depleted during the course of each half cycle. Note that this difference in fluxes does not imply an accumulation of a net negative charge during the cycle. This is because the right electrode is bombarded by an equal flux of negative ions (as opposed to positive ions) in the first half of the cycle followed by an equal flux of positive ions in the second half of the cycle. In other words, at any instant of the cycle, the flux of positive ions exiting the plasma at one electrode is equal to the flux of negative ions exiting the other electrode.

Figure 5 shows that the peak ion flux during a half cycle is comparable to twice the diffusion flux of the ions in the absence of a bias. The total flux of ions integrated over a full cycle is equivalent to the diffusion flux of ions without a bias potential. Therefore, for low bias frequencies, the flux of ions bombarding the electrode is independent of the magnitude of the applied bias potential and is limited by the ion diffusion flux. The only effect of the applied bias potential is to temporally redistribute this diffusion flux between the two elec-

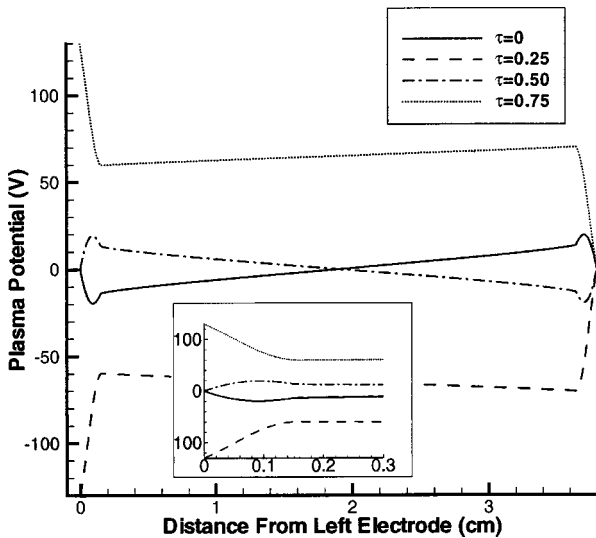


FIG. 6. Spatiotemporal evolution of the potential at base case conditions for a bias frequency of 10 MHz.

trodes. Instead of exiting both electrodes simultaneously, the positive ions exit only the negatively biased electrode while the negative ions exit only the positively biased electrode during each half cycle.

A closer examination of Fig. 5 shows a small phase lag between the ion flux and the applied potential which corresponds to the transit time of ions through the sheath. At this low frequency, the ion transit time is only a small fraction of the bias period (Table II). During this period, the electrode reverses polarity, and the sheath undergoes a transition from a net positive charge when the electrode is negatively biased, to a net negative charge when it is positively biased with respect to the bulk plasma. Since the time for this transition is short compared to the overall bias period, the charge in the sheath regions essentially remains monotonic in nature for each half cycle, i.e., either fully positive or fully negative. This is not true, however, when the bias frequency is increased.

### B. Intermediate frequencies ( $\nu_i < \omega < \omega_i$ )

As the bias frequency is increased beyond the collision frequency, temporal inertia of the ions starts to dominate over the collisional drag. The ion velocity, therefore, is no longer in equilibrium with the local electric field. In this regime, the bias frequency can approach the ion-plasma frequency. Physically, this represents the case when the transit time of ions through the sheath constitutes a significant fraction of the bias period.

Figure 6 shows the plasma potential profiles at various instants of the bias cycle for a bias frequency of 10 MHz. At this frequency, there is insufficient time for the applied bias potential to be fully shielded in the sheaths and a significant electric field exists in the bulk plasma. Therefore, the displacement current in the bulk plasma is greater than in the low frequency case (Fig. 1(b)). Its magnitude, however, is still smaller relative to the conduction current since most of the potential drop occurs in the sheaths rather than the bulk plasma. Interestingly, the potential profiles in the sheath re-

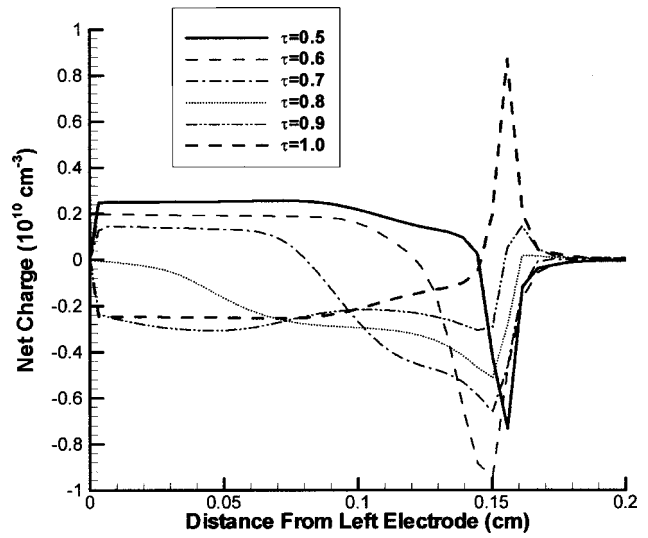


FIG. 7. Spatiotemporal evolution of net charge at base case conditions for a bias frequency of 10 MHz.

gions are no longer monotonic, but show the formation of potential wells near each electrode when the electrode changes polarity with respect to the bulk plasma (Fig. 6,  $\tau = 0$  and 0.5). This nonmonotonic sheath potential is related to the evolution of the charge distribution in the sheath.

Figures 7, 8, and 9 show the net charge density and the ion-density profiles in the sheath region near the left electrode. At  $\tau = 0.5$ , the electrode potential is zero with respect to the plasma center. However, due to the relatively long transit time of ions through the sheath, some positive ions continue to persist in the sheath (Fig. 8) while negative ions are unable to diffuse back to the electrode (Fig. 9). Therefore, a net positive charge exists for some region in the sheath ( $0 < x < 0.14$  cm) near the electrode at  $\tau = 0.5$  (Fig. 7). Beyond this point, there is a region of net negative charge ( $0.14 \text{ cm} < x < 0.18 \text{ cm}$ ) which is formed due to the inertia of positive ions as they continue to be accelerated from the bulk plasma towards the electrode even at  $\tau = 0.5$  when the elec-

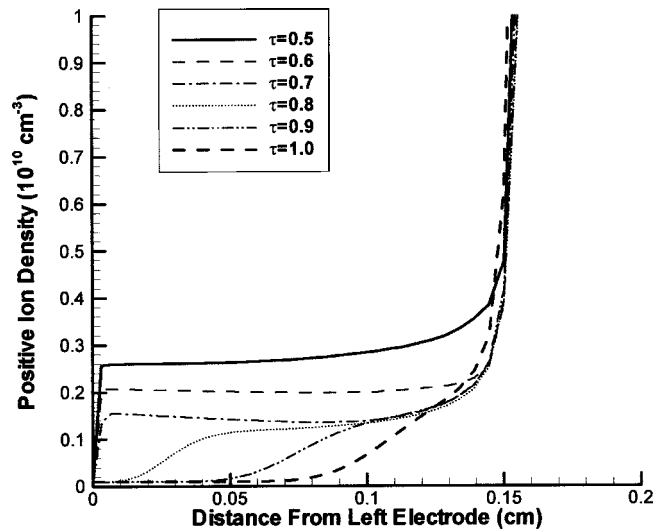


FIG. 8. Spatiotemporal evolution of positive ion density near left electrode at base case conditions for a bias frequency of 10 MHz.

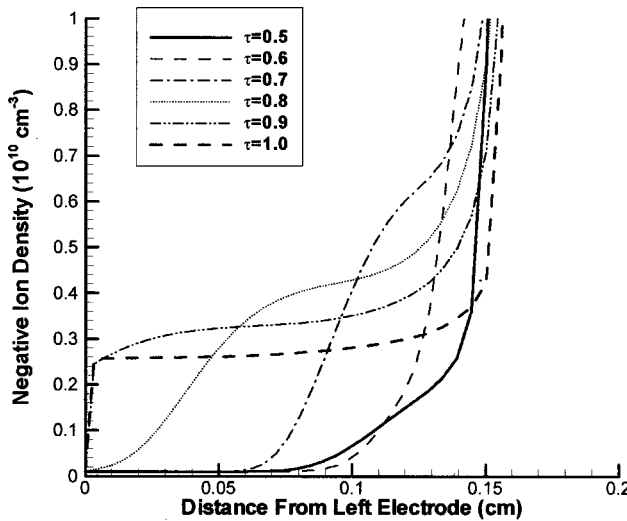


FIG. 9. Spatiotemporal evolution of negative ion density near left electrode at base case conditions for a bias frequency of 10 MHz.

trode potential is zero. The overall charge distribution in the sheath at  $\tau=0.5$ , therefore, consists of a double layer with positive charge near the electrode followed by a sharp negative charge spike at the sheath edge. This charge distribution is responsible for the formation of a “well” in the spatial potential profile in Fig. 6 at  $\tau=0.5$  and is indicative of a reversal in the direction of the electrostatic field in the sheath. The electric field is positive close to the electrode ( $0 < x < 0.1$  cm), and turns negative near the sheath edge ( $0.1 < x < 0.18$  cm). At even higher frequencies this develops into an oscillatory structure of the potential (see Sec. IV C).

After  $\tau=0.5$ , the left electrode becomes positively biased and attracts negative ions from the bulk plasma. Figure 9 shows that a significant period of time is required for the negative-ion front to traverse the length of the sheath and reach the electrode. The negative-ion front first advances during the period  $\tau=0.5\text{--}0.6$  as negative ions are attracted towards the electrode, but the velocity of the negative ions is still small. At later times, however, negative ions are accelerated and the velocity of the bottom end of the negative-ion front exceeds the velocity of the top end of the front. The negative-ion front, therefore, spreads as a function of time with the bottom end of the front advancing towards the electrode while the top end retreats as negative ions are depleted.

By about  $\tau=0.8$ , the negative-ion front first reaches the electrode (Fig. 9) while the positive ions near the electrode have been repelled (Fig. 8). A net negative charge exists throughout the entire length of the sheath at  $\tau=0.8$  (Fig. 7) indicating that the potential distribution is monotonic and the electric field is positive. The evolution of the plasma potential and the electric field in the sheath region, therefore, is clearly coupled with the transit time of the negative ions through the sheath region.

After  $\tau=0.75$ , the electrode bias is decreasing (in magnitude) with time, but the negative ions continue to be extracted from the bulk plasma due to ion inertia. The positive-ion front at  $x=0.15$  remains essentially stationary since the bias period is much shorter than the ion diffusion time (Fig. 8). As a result of inertia, the negative ions continue to over-

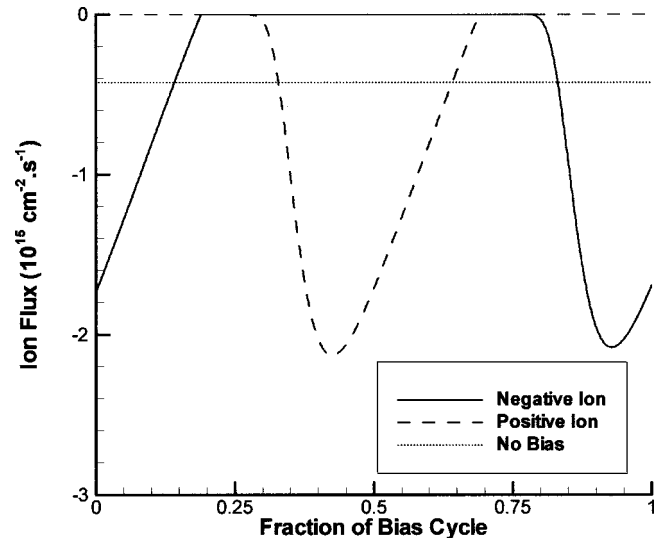


FIG. 10. Ion flux at the left electrode during a bias cycle at base case conditions for a bias frequency of 10 MHz.

shoot and a net positive charge is gradually formed at the edge of the sheath during the period  $\tau=0.8\text{--}1.0$  (Fig. 7). By  $\tau=1.0$ , an inverted double layer exists with a net negative charge near the electrode ( $0 < x < 0.14$  cm) and a net positive charge near the sheath edge ( $0.14 \text{ cm} < x < 0.18$  cm). This charge distribution is the inverse of the distribution which existed at the electrode at  $\tau=0.5$ . The overall evolution of the space charge during the course of a half cycle, therefore, describes a complete oscillation with the negatively charged region becoming positively charged and the positively charged region becoming negatively charged.

Figure 10 shows the evolution of the ion fluxes at the left electrode during the course of a bias cycle. The effect of the transit time of ions through the sheath is clearly evident in the evolution of fluxes. The positive-ion flux continues until  $\tau=0.7$  even when the electrode is positively biased with respect to the plasma. Negative-ion flux does not appear until  $\tau=0.8$  representing the transit time of the negative-ion fronts through the sheath. As opposed to the low frequency case, the ion flux is significantly greater than the corresponding diffusion flux without an applied bias potential. At this bias frequency, there is insufficient time for the applied bias potential to be fully shielded in the sheath regions. Due to the presence of these electric fields, therefore, the ion flux to the walls exceeds the diffusion flux in the bulk plasma. Consequently, a high bias frequency, approaching the (ion) plasma frequency is required to extract ions at a faster rate from the plasma.

### C. High frequency ( $\nu_i < \omega_i < \omega$ )

At operating frequencies beyond the ion-plasma frequency, the time period of the applied bias is significantly shorter than the transit time of ions through the sheath. Therefore, ions essentially oscillate back and forth in the sheath region and exit the sheath only after several bias cycles.

Figure 11 shows the plasma potential at various instants of the bias cycle for a bias frequency of 60 MHz. The spatial

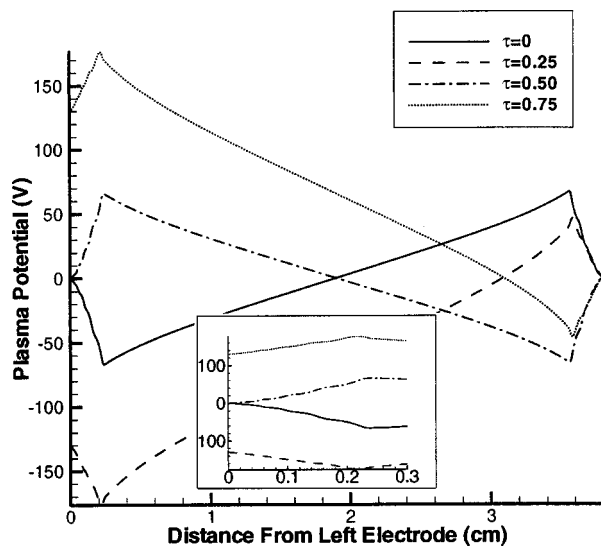


FIG. 11. Spatiotemporal evolution of the potential at base case conditions for a bias frequency of 60 MHz.

potential profile is highly nonmonotonic throughout the cycle since the applied potential is not shielded effectively in the sheaths. Since the potential drop in the sheaths is less than the potential drop in the bulk plasma, displacement current in the bulk plasma dominates over conduction current in this regime. The potential profile in the sheath regions also shows the presence of finer scale oscillations. These oscillations are related to the charge density profile in the sheath.

Figures 12, 13, and 14 show the evolution of the net charge density and the ion density profiles near the left electrode during the course of a half cycle. The evolution of charge-density profiles in the sheath region describes the propagation of a high-amplitude, plasma wave in a nonuniform plasma. These plasma waves are launched from the sheath edge corresponding approximately to the position where the bias frequency is equal to plasma frequency (Figs. 13 and 14,  $x=0.25$  cm). For spatial locations beyond this point, the plasma density and consequently the plasma fre-

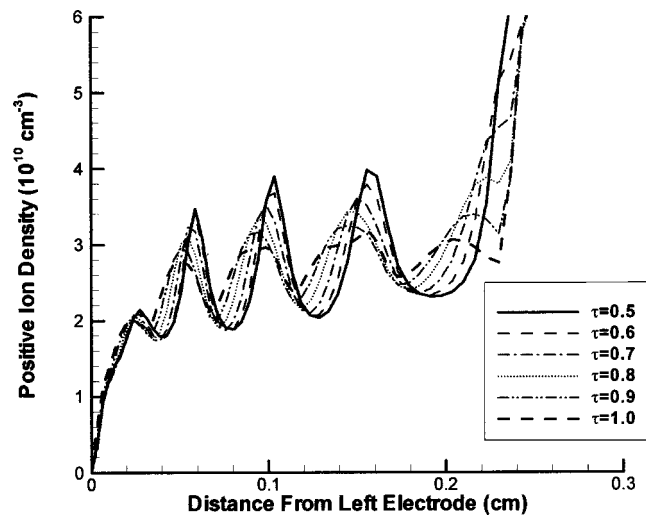


FIG. 13. Spatiotemporal evolution of positive ion density near left electrode at base case conditions for a bias frequency of 60 MHz.

quency increase sharply. Since the bias frequency is less than the plasma frequency corresponding to these spatial locations, the plasma waves are unable to propagate in the bulk plasma and are quickly damped within a few Debye lengths.

At  $\tau=0.5$ , the spatial profile of the ion densities in the sheath region shows several peaks and valleys (Figs. 13 and 14). This “bunching” of ions occurs during the course of several cycles as the ions are alternately attracted and then repelled away from the electrode. Similarly, the net charge-density profiles show alternate peaks of net positive and negative charge (Fig. 12). As a result of this charge profile, electrostatic fields are generated which tend to attract the negative-ion peaks towards the intermediate positive-ion peaks and the positive-ion peaks towards the negative-ion peaks. During the course of a half-cycle, ions migrate and overshoot due to ion inertia. By  $\tau=1.0$ , the charge density profile becomes the inverse of that at  $\tau=0.5$  (Fig. 12). The positive-ion density profile at  $\tau=1.0$  is similar to the negative-ion density profile at  $\tau=0.5$  while the negative-ion

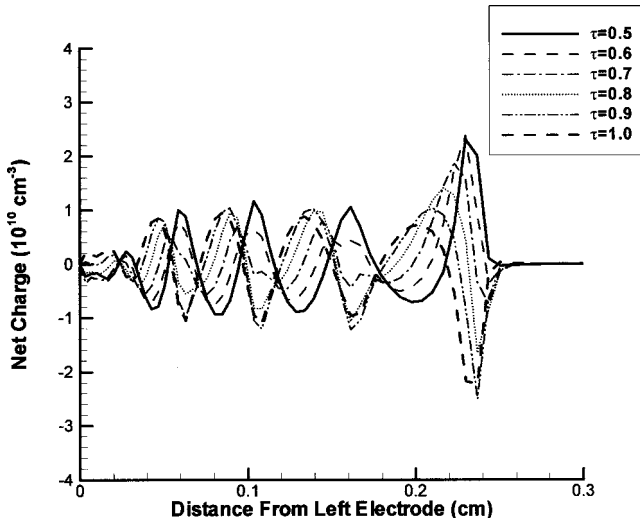


FIG. 12. Spatiotemporal evolution of net charge at base case conditions for a bias frequency of 60 MHz.

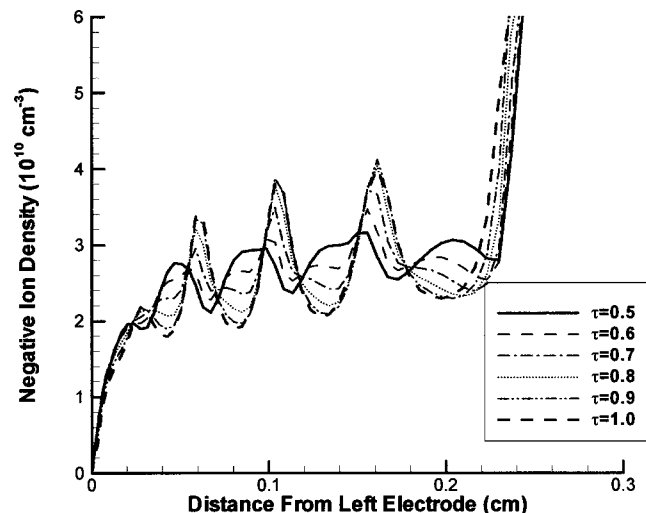


FIG. 14. Spatiotemporal evolution of negative ion density near left electrode at base case conditions for a bias frequency of 60 MHz.

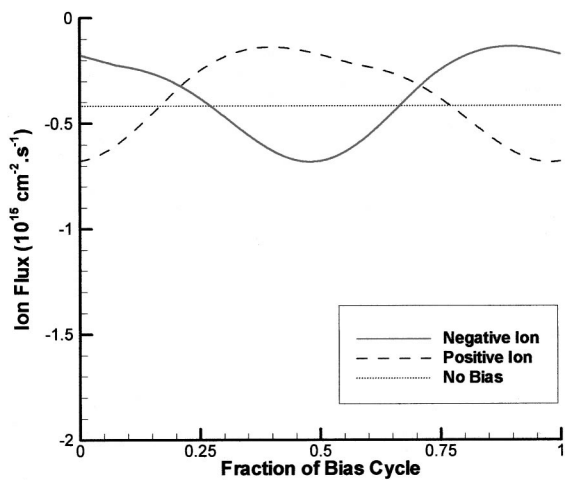


FIG. 15. Ion flux at the left electrode during a bias cycle at base case conditions for a bias frequency of 60 MHz.

density profile at  $\tau=1.0$  is similar to the positive-ion density profile at  $\tau=0.5$ . Overall, the positive-ion density profiles show a small net displacement towards the electrode in this half cycle (Fig. 13) while the negative ions are displaced away from the electrode (Fig. 14).

Figure 15 shows the evolution of the ion flux at the left electrode during a bias cycle. Since ions are no longer able to respond to the applied frequency, the perturbation in the ion velocities due to the applied bias is small. The ion fluxes, therefore, are only weakly modulated by the applied bias. The electrode is continuously bombarded by both positive and negative ions throughout the cycle with an average flux equal to the diffusion flux of ions. As a result of a net displacement towards the electrode, a peak in the negative-ion flux is formed around  $\tau=0.5$  while a peak in positive-ion flux is formed around  $\tau=1.0$ .

Based on the ion flux evolution at the electrode (Figs. 5, 10, and 15), operation in the intermediate frequency regime appears advantageous for rapidly extracting ions from the plasma at the conditions studied (Table I, 20 mTorr pressure and bias potential of 130 V). At low frequencies, alternate bombardment by positive ions and negative ions is possible but the ion flux is limited by the diffusion flux from the bulk plasma. In addition, if the bias period is comparable to the residence time of the charge on device features during plasma processing, the device will still have adequate time to charge during each half of the bias cycle. Therefore, charge damage and etch profile distortions may still occur during each half cycle of the pulse. Alternate bombardment of the electrode by positive and negative is also possible with intermediate values of the frequency, albeit with a finite phase lag with respect to the applied bias. There is less time for collisional drag to limit the ion flux at intermediate frequencies and ions may be extracted at a faster rate from the plasma compared to low frequencies. Furthermore, less time is available during each half cycle for charging and etch profile distortions to occur. Increasing the bias frequency beyond the ion plasma frequency, results in “trapping” of the ions (back and forth oscillations), and the ion flux at the

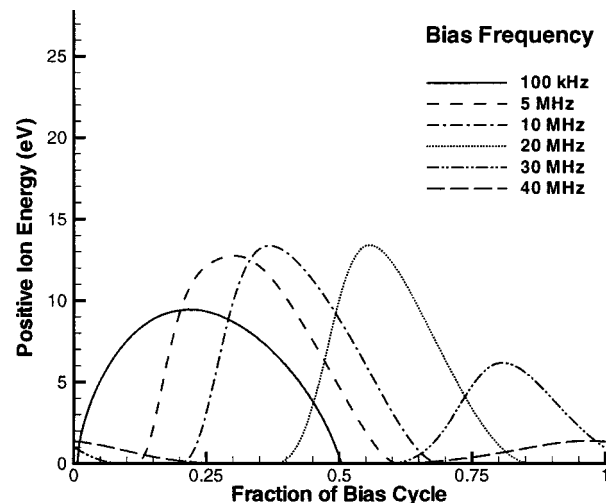


FIG. 16. Positive ion energy at the left electrode during a bias cycle for different values of bias frequency.

electrode is essentially reduced to the diffusion flux of the ions.

Another parameter critical for etching applications is the energy of the ions bombarding the electrode. Figure 16 shows the energy of the positive ions at the left electrode during the course of a bias cycle for different values of bias frequency. The energy of the negative ions is, of course, identical but it is shifted in phase by 180°. As in the case of the ion flux, the effect of the ion transit time is also apparent in the ion-energy evolution. At low frequencies (100 MHz) the ion energy essentially follows the applied bias while at intermediate frequencies (5–20 MHz), the ion energy lags the applied bias by the ion transit time. For frequencies less than  $\omega_i$  (5–20 MHz), the peak ion energy also increases with bias frequency as less time is available for collisional drag to retard ions in the sheath. At 30 MHz, the bias period is shorter than the ion transit time through the sheath and the positive ions reach the electrode when it is positively biased (i.e., repelling the positive ions), and the peak ion energy drops. Beyond this critical frequency, the peak ion energy drops rapidly (40 MHz) with increasing bias frequency and for a value of 60 MHz, the ion energy is essentially the thermal energy of ions (not shown). It is clear from this analysis that bias frequencies in the intermediate regime are optimal for extracting high energy ions out from the plasma, for the conditions studied.

In Fig. 16, the peak ion energy is significantly less than half the applied bias potential ( $V_b/2=65$  V). Half of the applied bias potential represents the maximum value of the ion energy if the applied potential is symmetrically distributed between the two electrodes. Since the ion mean free path at 20 mTorr is about 1 mm, while the sheath thickness is of the order of 2 mm, ions suffer on average of a couple of collisions in the sheath before striking the electrode. Similarly, due to the significant transit time of ions at intermediate frequencies, ions experience a decreasing bias potential as they accelerate through the sheath, resulting in lower ion energy. In order to increase the ion energy, therefore, it be-

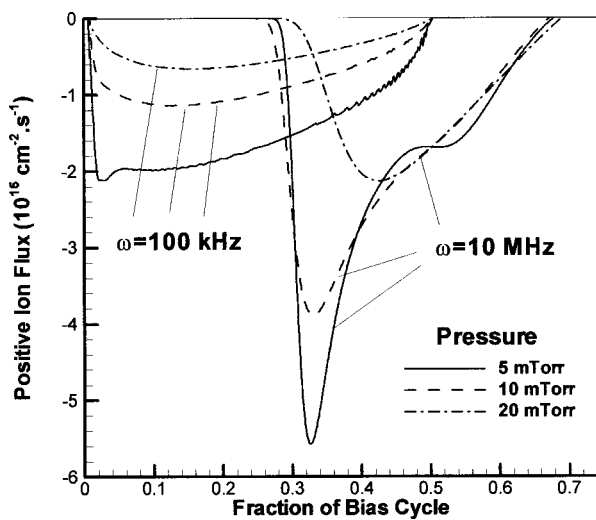


FIG. 17. Positive ion flux at the left electrode during a bias cycle for different pressures.

comes necessary to either increase the bias potential or decrease the operating pressure.

#### D. Effect of pressure

Figure 17 shows the positive-ion flux at the left electrode for different values of pressure at a low bias frequency (100 kHz) and an intermediate frequency (10 MHz). At low bias frequencies, the ion flux is limited by ion diffusion. Therefore at 100 kHz, the ion flux at the electrode increases proportionately as the collision frequency of the ions decreases with pressure (remember that the peak ion density is kept constant as pressure varies; in practice this can be achieved by also changing the power of the plasma that eventually turns into an ion-ion plasma). An increase in the peak value of the ion flux is also seen in the 10 MHz case as the pressure is reduced from 20 to 5 mTorr. At a pressure of 5 mTorr the ion mean free path is significantly greater than the sheath thickness and ion transport through the sheath becomes collisionless. The ion-flux profiles at both frequencies show oscillatory behavior. These oscillations represent the formation of waves (or bunches) in the ion-density profiles as the ions are trapped in potential wells when the electrodes reverse polarity. In contrast to the plasma waves shown earlier at high frequencies (60 MHz), which are formed mainly due to temporal inertia of ions (i.e., ions continue to overshoot in time), these low-frequency oscillations are mainly due to the spatial inertia of ions (i.e., ions overshoot in space). Similar oscillations in the ion flux profiles may also be observed in the numerical results of Kanakasabapathy and Overzet<sup>37</sup> who modeled the effects of a low frequency bias on highly electronegative plasmas under low pressure conditions.

Figure 18 shows the corresponding ion energies at the left electrode for different values of pressure. For both the low (100 kHz) and intermediate (10 MHz) frequency values, the ion energy increases as the pressure decreases and ion transport becomes less collisional. At higher values of pressure (20 and 10 mTorr), the peak energy of the ions extracted at 10 MHz is greater than the peak energy at 100 kHz. For

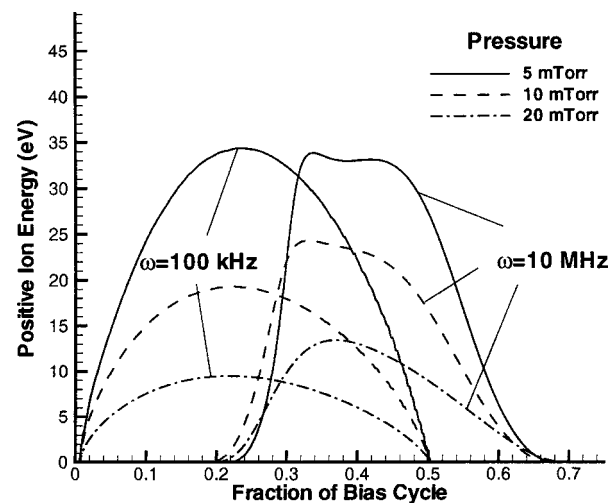


FIG. 18. Positive ion energy at the left electrode during a bias cycle for different pressures.

these pressures, the greater collisional drag at low frequencies dominates over the effect of ion transit time at higher frequencies. At low pressures (5 mTorr), however, the effect of the ion transit time becomes more significant, and the peak ion energies are comparable at the two frequencies. Therefore, extraction of high energy ions at high pressures is favored by higher bias frequencies whereas at low pressures lower bias frequencies become more favorable.

#### E. Effect of bias potential

Figure 19 shows the ion flux at the left electrode for different values of the applied bias potential. At low bias frequencies (100 kHz), the ion flux is effectively limited by ion diffusion and is nearly independent of the applied bias potential. At intermediate frequencies (10 MHz), when the bias period is less than the characteristic collision time, the ion flux shows a small increase as the bias potential increases. In contrast, the ion energy at the electrode shows significant increase at both frequencies as the bias potential

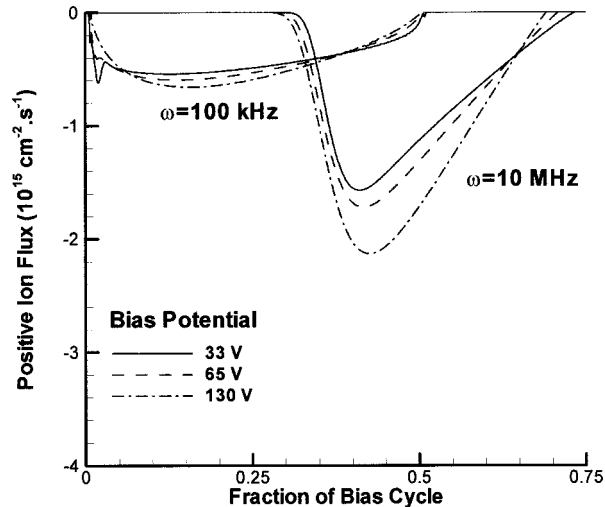


FIG. 19. Positive ion flux at the left electrode during a bias cycle for different bias potentials.

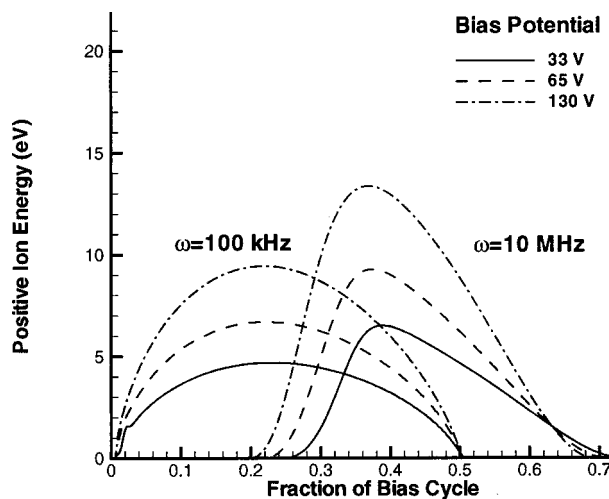


FIG. 20. Positive ion energy at the left electrode during a bias cycle for different bias potentials.

is increased (Fig. 20). The increase in ion energy, however, is not proportional to the applied bias potential because collisional drag also increases with ion velocity. It may also be noted that despite a significant increase in ion velocity, the transit time of the ions through the sheath (at 10 MHz) is only weakly affected. This indicates that the increase in ion velocity is effectively offset by a corresponding increase in sheath length as the bias potential increases. The estimate for the ion transit time being approximately the ion plasma frequency, therefore, suffices for all values of bias potential significantly greater than the ion temperature.

## V. CONCLUSIONS AND RECOMMENDATIONS

A one-dimensional fluid model was developed to simulate the effect of a radio frequency bias applied to a positive ion-negative ion (ion-ion or electronless) plasma. The ion continuity and momentum equations were coupled to the Poisson equation for the electric field. Ion-ion plasmas show significantly different behavior compared to conventional electron-ion plasmas.

(1) In contrast to conventional electron-ion plasmas, the plasma potential is not the most positive potential in an ion-ion plasma. For low bias frequencies compared to the ion collision frequency, the potential distribution between the electrodes is monotonic, much like in electrochemical systems. For equal masses and temperatures of the positively and negatively charged species, the applied bias potential is distributed symmetrically between the electrodes.

(2) Each electrode reverses polarity with respect to the bulk plasma during a bias period. Consequently, the net charge in the sheath also changes polarity with a net negative charge existing in the sheath for an equal duration as a net positive charge. This is in contrast to electron-ion plasmas in which the sheath always has a net positively charge.

(3) Due to the lower temperature and greater mass of negative ions compared to electrons, the sheath structure in ion-ion plasmas changes significantly as the rf bias frequency is varied. For low bias frequencies (100 kHz), the charge distribution is monotonic during each half cycle. For

intermediate frequencies (10 MHz), when the bias period approaches the ion transit time through the sheath, double layers form with both positive and negative charges coexisting in the sheath. For frequencies beyond the (ion) plasma frequency (60 MHz), plasma waves are launched from the sheath edge, and the sheath contains multiple peaks of positive and negative charge (multiple double layers).

(4) For a relatively large range of bias frequencies (up to the plasma frequency), each electrode is bombarded alternately by high energy positive and negative ions during a rf bias cycle. This alternate bombardment by positive and negative ions may help alleviate charging and notching effects associated with electron-ion plasmas. For bias frequencies greater than the plasma frequency, however, the electrode is bombarded simultaneously by low energy positive and negative ions with ions energies approaching the thermal value.

(5) At low bias frequencies, the peak ion flux in a rf cycle is limited by ion diffusion and is independent of the applied bias potential. The peak ion flux may be increased by lowering the pressure or by using a bias frequency approaching the ion plasma frequency.

(6) The ion energy increases with the applied bias potential. At relatively high pressures (20 mTorr), the ion energy at low frequencies (100 kHz) is limited by collisions. The peak ion energy may then be increased by using a higher bias frequency (10 MHz). At lower pressures, however, the effect of collisions is mitigated while the effect of ion transit time becomes significant as the bias frequency increases. In this case, a lower bias frequency (100 s kHz) is favorable for extracting high energy ions from the plasma.

## ACKNOWLEDGMENTS

The authors are grateful to the National Science Foundation (CTS-9713262) and the State of Texas (Texas Advanced Technology Program) for financial support. Many thanks to Dr. I. D. Kaganovich, Dr. V. Mani, and B. Ramamurthi for helpful technical discussions throughout this work.

<sup>1</sup> V. Midha and D. J. Economou, *Plasma Sources Sci. Technol.* **9**, 256 (2000).

<sup>2</sup> I. Kaganovich, D. J. Economou, B. N. Ramamurthi, and V. Midha, *Phys. Rev. Lett.* **84**, 1918 (2000); I. Kaganovich, B. N. Ramamurthi, and D. J. Economou, *Phys. Rev. E* (submitted).

<sup>3</sup> A. Smith and L. J. Overzet, *Plasma Sources Sci. Technol.* **8**, 82 (1999).

<sup>4</sup> M. V. Malyshev, V. M. Donnelly, J. I. Colonell, and S. Samukawa, *J. Appl. Phys.* **86**, 4813 (1999).

<sup>5</sup> S. A. Gutsev, A. A. Kudryavtsev, and V. A. Romanenko, *Tech. Phys.* **40**, 1131 (1995).

<sup>6</sup> D. Smith, A. G. Dean, and N. G. Adams, *J. Phys. D* **7**, 1944 (1974).

<sup>7</sup> W. L. Fite and J. A. Rutherford, *Discuss. Faraday Soc.* **37**, 192 (1964).

<sup>8</sup> L. J. Puckett and W. C. Lineberger, *Phys. Rev. A* **1**, 1635 (1970).

<sup>9</sup> G. A. Woosley, I. C. Plump, and D. B. Lewis, *J. Phys. D* **6**, 1883 (1973).

<sup>10</sup> H. Amemiya, *Dusty and Dirty Plasmas, Noise, and Chaos in Space and in the Laboratory*, edited by H. Kikuchi (Plenum, New York, 1994).

<sup>11</sup> J. Newman, *Electrochemical Systems* (Prentice-Hall, Engelwood Cliffs, NJ, 1973).

<sup>12</sup> H. Amemiya, *J. Phys. D* **23**, 999 (1990).

<sup>13</sup> I. D. Kaganovich and L. D. Tsendin, *Plasma Phys. Rep.* **19**, 645 (1993).

<sup>14</sup> L. D. Tsendin, *Sov. Tech. Phys.* **34**, 11 (1989).

<sup>15</sup> M. A. Lieberman and A. J. Lichtenberg, in *Principles of Plasma Discharges and Materials Processing* (Wiley, New York, 1994), p. 137.

<sup>16</sup> A. J. Lichtenberg, I. G. Kouznetsov, Y. T. Lee, M. A. Lieberman, I. D.

- Kaganovich, and L. D. Tsendin, *Plasma Sources Sci. Technol.* **6**, 437 (1997); A. J. Lichtenberg, V. Vahedi, M. A. Lieberman, and T. Ronglien, *J. Appl. Phys.* **75**, 2339 (1994).
- <sup>17</sup>V. I. Kolobov and D. J. Economou, *Appl. Phys. Lett.* **72**, 656 (1998).
- <sup>18</sup>I. G. Kouznetsov, A. J. Lichtenberg, and M. A. Lieberman, *J. Appl. Phys.* **86**, 4142 (1999).
- <sup>19</sup>A. Kono, *J. Phys. D* **32**, 1357 (2000).
- <sup>20</sup>R. N. Franklin and J. Snell, *J. Phys. D* **33**, 1 (2000).
- <sup>21</sup>L. J. Overzet, Y. Lin, and L. Luo, *J. Appl. Phys.* **72**, 5579 (1992).
- <sup>22</sup>S. Samukawa and T. Mieno, *Plasma Sources Sci. Technol.* **5**, 132 (1996).
- <sup>23</sup>T. Shibayama, H. Shindo, and Y. Horiike, *Plasma Sources Sci. Technol.* **5**, 254 (1996).
- <sup>24</sup>T. H. Ahn, K. Nakamura, and H. Sugai, *Plasma Sources Sci. Technol.* **5**, 139 (1996).
- <sup>25</sup>G. S. Hwang and K. P. Giapis, *Phys. Rev. Lett.* **79**, 845 (1997).
- <sup>26</sup>M. B. Hopkins and K. N. Mellon, *Phys. Rev. Lett.* **67**, 449 (1991).
- <sup>27</sup>D. Hayashi and K. Kadota, *J. Appl. Phys.* **83**, 697 (1998).
- <sup>28</sup>W. Swider, *Ionospheric Modeling* (Birkhauser, Basel, 1988).
- <sup>29</sup>D. P. Lymberopoulos and D. J. Economou, *J. Appl. Phys.* **73**, 3668 (1993).
- <sup>30</sup>D. B. Graves, *J. Appl. Phys.* **62**, 88 (1987).
- <sup>31</sup>T. J. Sommerer and M. J. Kushner, *J. Appl. Phys.* **71**, 1654 (1991).
- <sup>32</sup>M. Meyyappan and T. R. Govindan, *J. Vac. Sci. Technol. A* **10**, 1344 (1992).
- <sup>33</sup>F. F. Chen, *Introduction to Plasma Physics and Controlled Fusion, Plasma Physics*, 2nd ed. (Plenum, New York, 1984), Vol. 1.
- <sup>34</sup>M. A. Barnes, T. J. Cotler, and M. A. Elta, *J. Comp. Phys.* **77**, 53 (1988).
- <sup>35</sup>A. C. Hindmarsh, Lawrence Livermore Lab. Report UCRL-87406 (1982); UCRL-89311 (1983); A. C. Hindmarsh, in *Scientific Computing*, edited by R. S. Stepleman (North Holland, Amsterdam, 1983), p. 55.
- <sup>36</sup>S. K. Kanakasabapathy, L. J. Overzet, V. Midha, and D. J. Economou, *Appl. Phys. Lett.* **78**, 22 (2001).
- <sup>37</sup>S. K. Kanakasabapathy and L. J. Overzet, *J. Vac. Sci. Technol.* (accepted for publication).